Photocatalytic Route for Synthesis of Hollow Porous Carbon/Pt Nanocomposites with Controllable Density and Porosity†

Yun Hau Ng,‡ Shigeru Ikeda,*,‡ Takashi Harada,‡ Sangin Park,‡ Takao Sakata,§ Hirotaro Mori,§ and Michio Matsumura‡

Research Center for Solar Energy Chemistry, Osaka University, 1-3 Machikaneyama, Toyonaka 560-8531, Japan, and Research Center for Ultra-High Voltage Electron Microscopy, Osaka University, 7-1 Mihogaoka, Ibaraki 567-0047, Japan

Received July 26, 2007. Revised Manuscript Received October 31, 2007

Simultaneous photoreduction of Pt(IV) ions and photooxidative polymerization of phenol on the surface of titanium(IV) oxide (TiO_2) under ultraviolet light irradiation induced the formation of a composite, Pt-loaded TiO_2 covered with a layer of phenolic polymer. Subsequent carbonization of the polymer layer and removal of TiO_2 core particles yielded hollow carbon incorporated with platinum nanoparticles (*n*Pt@*h*C). By varying the photoirradiation time, appreciable changes in density and porosity of the polymer layer and the carbon shell in *n*Pt@*h*C were observed: prolonged irradiation induced a densification of the carbon matrix, resulting in a decrease in pore volume. Mainly due to the modulation of active surface of Pt nanoparticles, the densification of carbon was found to influence catalytic activity for hydrogenation of normal olefins.

Introduction

Porous carbon materials have recently been the focus of intense study, especially in the field of catalysis as a support material owing to their promising properties such as high surface area, high stability in acidic and basic media, and controllable porosity.[1–3] The most efficient approach utilized for preparing these porous carbons is the templating method, in which silica-based porous materials or colloidal crystals are mainly used as sacrificial molds. The availability of a wide variety of materials, such as zeolites, MCM-48, SBA-15, and colloidal silica, provides vast opportunities for the synthesis of porous carbon with various imprinted structures.[4–6]

The basic strategy of this method is filling the solid template with a carbon precursor, e.g., glucose, sucrose, pitch, or furfuryl alcohol, followed by carbonization of the resulting composite and dissolution of the template by chemical etching. Hence, by the selection of appropriate carbon precursors, silica-based templates, and carbonization settings, e.g., temperature and gas medium, various carbon materials with different degree of porosity, graphitization, and density can be obtained through the method.[7–9] Indeed, there are many examples in the literature for better control of such structural properties of carbons. However, the ability for fine-tuning to yield carbon materials with promising properties still remains a desirable research goal that has not been fully explored.

Besides efficient control of the structural properties of carbons themselves, fabrication of metal−carbon composites is another important subject for their application, especially in the field of catalysis. Loading of these metals on carbon materials generally involves a multistep process, i.e., post-loading of the respective metal ions onto carbons followed by reduction of them in a hydrogen atmosphere. Thus, a rather simplified fabrication method to prepare carbon−metal composites with well-defined structures has recently been formulated.

Recently, we have proposed an alternative method for preparing porous hollow carbon encapsulating Pt nanopar-

† Part of the "Templated Materials Special Issue".

* Corresponding author: phone +81-6-6850-6696; fax +81-6-6850-6699; e-mail sikeda@chem.es.osaka-u.ac.jp.

‡ Research Center for Solar Energy Chemistry.

§ Research Center for Ultra-High Voltage Electron Microscopy.

(1) (a) Ma, Z.; Kyotani, T.; Liu, Z.; Terasaki, O.; Tomita, A. *Chem. Mater.* **2001**, *13*, 4413. (b) Wang, J. N.; Zhang, L.; Niu, J. J.; Yu, F.; Sheng, Z. M.; Zhao, Y. Z.; Chang, H.; Pak, C. *Chem. Mater.* **2007**, *19*, 453. (c) Yang, Z.; Xia, Y.; Mokaya, R. *J. Am. Chem. Soc.* **2007**, *129*, 1673. (d) Lu, A.; Li, W.; Salabas, E.; Spliethoff, B.; Schuth, F. *Chem. Mater.* **2006**, *18*, 2086. (e) Ikeda, S.; Ishino, S.; Harada, T.; Okamoto, N.; Sakata, T.; Mori, H.; Kuwabata, S.; Torimoto, T.; Matsumura, M. *Angew. Chem., Int. Ed.* **2006**, *45*, 7063.

(2) (a) Toda, M.; Takagaki, A.; Okamura, M.; Kondo, J. N.; Hayashi, S.; Domen, K.; Hara, M. *Nature (London)* **2005**, *438*, 178. (b) Okamura, M.; Takagaki, A.; Toda, M.; Kondo, J. N.; Domen, K.; Tatsumi, T.; Hara, M.; Hayashi, S. *Chem. Mater.* **2006**, *18*, 3039. (c) Wang, X.; Liu, R.; Waje, M. M.; Chen, Z.; Yan, Y.; Bozhilov, K. N.; Feng, P. *Chem. Mater.* **2007**, *19*, 2395.

(3) (a) Xia, Y.; Yang, Z.; Mokaya, R. *Chem. Mater.* **2006**, *18*, 140. (b) Yu, C.; Fan, J.; Tian, B.; Zhao, D.; Stucky, G. D. *Adv. Mater.* **2002**, *14*, 1742. (c) Lee, J. S.; Joo, S. H.; Ryoo, R. *J. Am. Chem. Soc.* **2002**, *124*, 1156. (d) Lu, A.; Schmidt, W.; Spliethoff, B.; Schueth, F. *Adv. Mater.* **2003**, *15*, 1602.

(4) Kyotani, T.; Ma, Z.; Tomita, A. *Carbon* **2003**, *41*, 1451.

(5) (a) Lee, J.; Kim, J.; Hyeon, T. *Adv. Mater.* **2006**, *18*, 2073. (b) Ryoo, R.; Joo, S. H.; Kruk, M.; Jaroniec, M. *Adv. Mater.* **2001**, *13*, 677.

(6) Gierszal, K. P.; Jaroniec, M. *J. Am. Chem. Soc.* **2006**, *128*, 10026.

(7) (a) Delhaes, P. *Carbon* **2002**, *40*, 641. (b) Jeong, H. J.; Park, H. D.; Lee, J. D.; Park, J. O. *Carbon* **1996**, *34*, 417.

(8) (a) Yoon, S. B.; Chai, G. S.; Kang, S. K.; Yu, J. S.; Gierszal, K. P.; Jaroniec, M. *J. Am. Chem. Soc.* **2005**, *127*, 4188. (b) Gierszal, K. P.; Kim, T. W.; Ryoo, R.; Jaroniec, M. *J. Phys. Chem. B* **2005**, *109*, 23263.

(9) (a) Arriagada, R.; Bello, G.; Garcia, R.; Rodriguez-Reinoso, F.; Sepulveda-Escribano, A. *Microporous Mesoporous Mater.* **2005**, *81*, 161. (b) Lei, S.; Miyamoto, J.; Ohba, T.; Kanoh, H.; Kaneko, K. *J. Phys. Chem. C* **2007**, *111*, 2459.

10.1021/cm702034w CCC: $40.75
Published on Web 12/04/2007

ticles (*n*Pt@*h*C) by using photocatalytic reaction on titanium(IV) oxide (TiO_2) particles.[10] The principle of the fabrication is based on the redox ability of photoirradiated TiO_2 nanoparticles to induce simultaneous photoreduction of Pt(IV) ions and photooxidative polymerization of phenol, which eventually result in Pt-loaded TiO_2 covered by a phenolic polymer. This methodology enables loading of Pt nanoparticles and coverage of the carbon precursor on the TiO_2 template in a one-step process, and subsequent carbonization of the polymer layer and removal of TiO_2 yield the *n*Pt@*h*C composite. One of the significant aspects of *n*Pt@*h*C thus-obtained was that it works as an efficient catalyst for hydrogenation of various olefins.

It was also shown in our previous report that polymerization of phenol seemed to proceed even after the surface of TiO_2 was fully covered after photoirradiation for a certain period, while this was not clearly stated at the preceding stage. In subsequent study of the system, however, we found that this phenomenon induced remarkable alterations in properties of the thus-derived carbon shells. In the present study, therefore, we investigated in detail the effect of photoirradiation time on structural characteristics of the phenolic polymer covered on the TiO_2 surface and thus-derived *n*Pt@*h*Cs composite. The correlation of structures of *n*Pt@*h*Cs with their catalytic functions for hydrogenation of olefins was also examined.

Experimental Section

Preparation of Materials. An anatase TiO_2 powder supplied by Ishihara Sangyo (ST-21, average particle size 20 nm, BET surface area 50 $m^2\ g^{-1}$) was used throughout this study. In a typical procedure, 500 mg of ST-21 powder was dispersed in 400 cm^3 aqueous solution containing 200 mg of phenol and 7.7 μmol of hexachloroplatinic acid (H_2PtCl_6). The amount of H_2PtCl_6 added corresponds to 0.3 wt % TiO_2 as Pt metal. The suspension was then evacuated several times in a quartz inner-irradiation-type vessel connected to a closed gas circulation and evacuation system to ensure complete air removal. Photoirradiation of the suspension was performed with a high-pressure Hg lamp (450 W) under a reduced-pressure argon (Ar) atmosphere (30 kPa) at 293 K. The brownish samples obtained after the photoirradiation for various periods were retrieved by filtration, washed with 2 dm^3 distilled water to remove excessive phenol, and dried at 353 K in air to yield Pt-loaded TiO_2 covered with a phenolic polymer (Poly/Pt/TiO_2). The Poly/Pt/TiO_2 samples were then subjected to carbonization at 973 K for 6 h in vacuum followed by immersion of the samples in 10 cm^3 of 50% hydrofluoric acid (HF) for 24 h at room temperature to remove the TiO_2 cores. (*Caution: HF is highly corrosive and must be handled with care!*) Finally, the black powders were washed several times with acetone and dried at 353 K to produce *n*Pt@*h*C powders. Poly/Pt/TiO_2 and *n*Pt@*h*C samples obtained with different photoirradiation times were designated as Poly/Pt/TiO_2(photoirradiation time) and *n*Pt@*h*C(photoirradiation time), respectively; e.g., samples prepared with 1 h photoirradiation are designated as Poly/Pt/TiO_2(1) and *n*Pt@*h*C(1).

Characterization of Materials. The amount of hydrogen gas (H_2) generated from the suspension during photoirradiation was measured at certain time intervals by using a Shimadzu GC-8A gas chromatograph equipped with a MS-5A column (GL Sciences) and a TCD detector. The amount of polymer attached on the TiO_2 particles was measured by thermogravimetry (TG) analysis using a Bruker 2000A TG-DTA in air from room temperature to 873 K, with a heating ramp of 5 K min^{-1}. The polymer species was characterized by Fourier transform infrared (FT-IR) spectroscopy on a Nicolet 470 FT-IR spectrometer equipped with a MCT detector using a KBr disk technique. Typically, 2 mg of Poly/Pt/TiO_2 was ground with 198 mg of KBr to a fine powder. The mixture powders were then pressurized to form a KBr disk containing 1 wt % dispersed sample. Microscopic features of the samples were observed using a Hitachi H-9000 transmission electron microscope (TEM). Surface and pore analyses of *n*Pt@*h*C were performed by using a Quantachrome AUTOSORB-1 automated gas sorption system employing Ar as an adsorbate after pretreatment of the sample at 473 K for 2 h. The content of Pt in *n*Pt@*h*C was determined by inductively coupled plasma (ICP) analysis on a Perkin-Elmer OPTIMA 3000-XL ICP emission spectrometer. For the ICP analysis, *n*Pt@*h*C samples were immersed in aqua regia for 2 h to dissolve the Pt particles. The undissolved carbon particles were filtered by using a Millipore syringe-driven membrane filter. The clear solution was then diluted to an appropriate concentration before the measurement. The amount of CO irreversibly held (CO_{irr}) on the surface of Pt nanoparticles in *n*Pt@*h*C was measured by the pulse CO adsorption experiment. Prior to the measurement, the sample was treated in H_2 flow (10 $cm^3\ min^{-1}$) at 623 K for 30 min and flushed with helium flow (30 $cm^3\ min^{-1}$) for 30 min at the same temperature. After the temperature was cooled to room temperature, CO pulses were injected. The amount of adsorbed CO was determined using a Shimadzu GC-14B gas chromatograph equipped with an active carbon column and a TCD detector.

Catalytic Activity Measurement. Catalytic hydrogenation was conducted in a glass tube equipped with a H_2-filled balloon. Certain amounts of *n*Pt@*h*C (corresponding to 0.08 μmol of Pt), 1 mL of ethanol, and 0.5 mmol of substrate (1-hexene, 1-decene, or 1-hexadecene) were put into the glass tube and connected to the H_2-filled balloon. After three vacuum/H_2 cycles to replace air inside the reaction tube with H_2, the mixture of the substrate and *n*Pt@*h*C in EtOH was stirred at room temperature for 30 min. After centrifugal separation of *n*Pt@*h*C at 2330*g* for 10 min, the solution was injected into a Shimadzu GC 2010 gas chromatograph equipped with a flame ionization detector and a TC-FFAP capillary column to determine the amounts of substrates and products. The *n*Pt@*h*C sample retrieved from centrifugation was washed three times in ethanol and reused in 1-decene hydrogenation using the same procedures as described above. The *n*Pt@*h*C composite after reaction was characterized by TEM to study the stability of the structure.

Results and Discussion

Photocatalytic Polymerization of Phenol in Various Photoirradiation Times. Because of the low catalytic ability of a bare TiO_2 surface for reduction of H_2O, photogenerated e^- in TiO_2 was initially utilized for reduction of H_2PtCl_6 to form Pt deposits when an aqueous suspension containing TiO_2, H_2PtCl_6, and phenol was irradiated by light with energy greater than the band gap of TiO_2. After the formation of Pt metal on TiO_2, the photogenerated e^- was then consumed to reduce H_2O on the deposited Pt metal to a gaseous product

(10) Ng, Y. H.; Ikeda, S.; Harada, T.; Higashida, S.; Sakata, T.; Mori, H.; Matsumura, M. *Adv. Mater.* **2007**, *19*, 597.

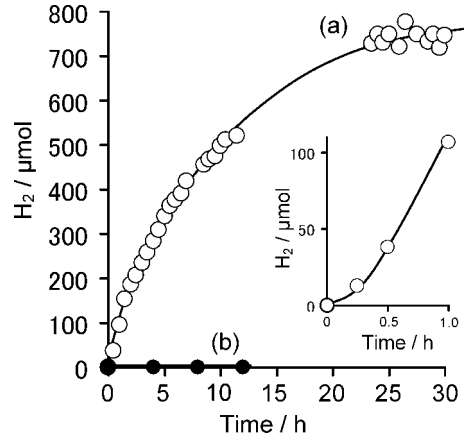

Figure 1. Time−course curves of H_2 liberation from an aqueous solution containing phenol, H_2PtCl_6, and TiO_2 (open circles) or Al_2O_3 (filled circles) under UV irradiation. The inset shows the initial rate of H_2 liberation from the TiO_2 system.

of H_2 (Figure 1a).[11] Because of these processes, an appreciable induction period was observed on the time course curves of H_2 liberation in the initial 30 min photoirradiation, as shown in the inset of Figure 1. On the other hand, photogenerated h^+ was likely to be instantly consumed in the oxidation of phenol: the color of TiO_2 particles became pale brown immediately after 15 min photoirradiation, indicating the deposition of polymeric compounds on the surface as a result of oxidative polymerization of phenol (see below). On the basis of the fact that neither liberation of H_2 nor changes in the color of particles were observed when reference systems using photocatalytically inert oxides such as Al_2O_3 instead of TiO_2 were performed (Figure 1b), observed reactions were confirmed to proceed as a result of redox reaction on TiO_2.

Prolonged photoirradiation induced change in the color of TiO_2 particles to deep brownish accompanied by a gradual decrease in rate of H_2 liberation, as shown in Figure 1a. This suggests an increase in the amount of polymeric compounds attached on the TiO_2 particles: subsequent surface coverage of polymeric compounds reduced available active site(s), resulting in a decrease in the rate of H_2 liberation. In order to obtain quantitative information of these compounds on the surface of TiO_2, TG measurements were carried out for the TiO_2 samples after photoirradiation for various periods (Poly/Pt/TiO_2), and the results are shown in Figure 2. As a reference, the result for bare TiO_2 is also shown in this figure. While the TG curve of bare TiO_2 only showed a slight weight loss below 150 °C attributable to dehydration and desorption of water, all of the Poly/Pt/TiO_2 samples exhibited an additional large weight loss between ca. 200 and 500 °C in the TG curves. Since the weight loss was accompanied by a major exothermic event starting at ca. 200 °C in the DTA curve (data not shown), it was ascribed to combustion of

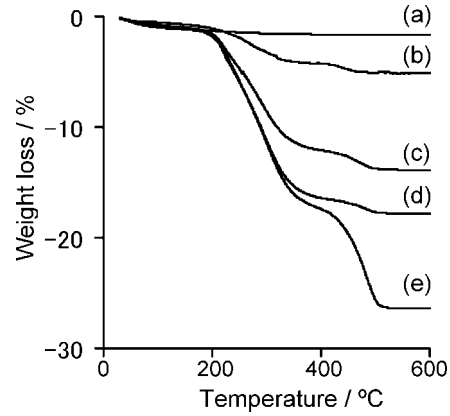

Figure 2. TG curves of (a) original TiO_2, (b) Poly/Pt/TiO_2(1), (c) Poly/Pt/TiO_2(2.5), (d) Poly/Pt/TiO_2(12), and (e) Poly/Pt/TiO_2(30).

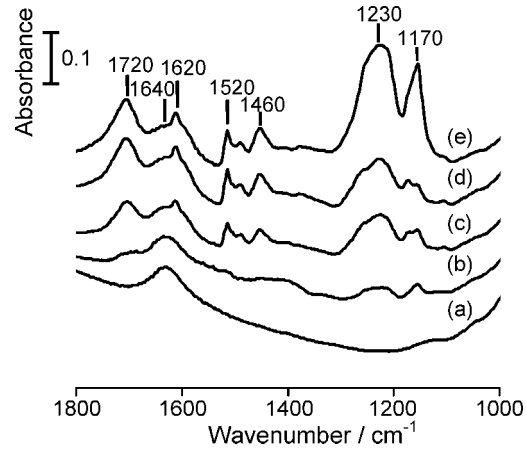

Figure 3. FTIR spectra of (a) original TiO_2, (b) Poly/Pt/TiO_2(1), (c) Poly/Pt/TiO_2(2.5), (d) Poly/Pt/TiO_2(12), and (e) Poly/Pt/TiO_2(30).

surface-covered organic components on TiO_2. Hence, when the remaining powder above 500 °C is assumed to be composed of TiO_2 and a very small amount of Pt deposits, the weight loss represents the amount of polymeric compounds on TiO_2. Among the samples examined, it is clear that the total amount of polymeric compounds increased in proportion to photoirradiation time: polymeric compounds included in Poly/Pt/TiO_2(1), Poly/Pt/TiO_2(2.5), Poly/Pt/TiO_2(12), and Poly/Pt/TiO_2(30) samples are estimated to be ca. 5%, 14%, 18%, and 26%, respectively. Another notable point is that all of the TG curves of Poly/Pt/TiO_2 samples exhibited analogous decomposition profiles comprised of two-step degradation starting at ca. 200 and 400 °C. Because of the similarity of these profiles to the decomposition profile of a phenolic polymer,[12] the surface-covered polymeric compound is likely to be an analogue(s) of this polymer, as expected from the above-described photocatalytic redox mechanism.

FT-IR spectra of Poly/Pt/TiO_2 samples obtained using 200 mg of KBr discs containing 1 wt % Poly/Pt/TiO_2 exhibit several identical absorption bands in addition to the absorption band at 1640 cm^{-1} assigned to the OH bending mode of adsorbed water on TiO_2 (Figure 3), indicating that the TiO_2 surfaces were covered by almost the same organic

(11) (a) Ohtani, B.; Ogawa, Y.; Nishimoto, S.-I. *J. Phys. Chem. B* **1997**, *101*, 3746. (b) Kraeutler, B.; Bard, A. J. *J. Am. Chem. Soc.* **1978**, *100*, 4317. (c) Kawai, T.; Sakata, T. *J. Chem. Soc., Chem. Commun.* **1980**, 694. (d) Yamaguti, K.; Sato, S. *J. Phys. Chem.* **1985**, *89*, 5510. (e) Ikeda, S.; Sugiyama, N.; Murakami, S.-Y.; Kominami, H.; Kera, Y.; Noguchi, H.; Uosaki, K.; Torimoto, T.; Ohtani, B. *Phys. Chem. Chem. Phys.* **2003**, *5*, 778. (f) Abe, R.; Sayama, K.; Sugihara, H. *J. Phys. Chem. B* **2005**, *109*, 16052.

(12) Uyama, H.; Maruichi, N.; Tonami, H.; Kobayashi, S. *Biomacromolecules* **2002**, *3*, 187.

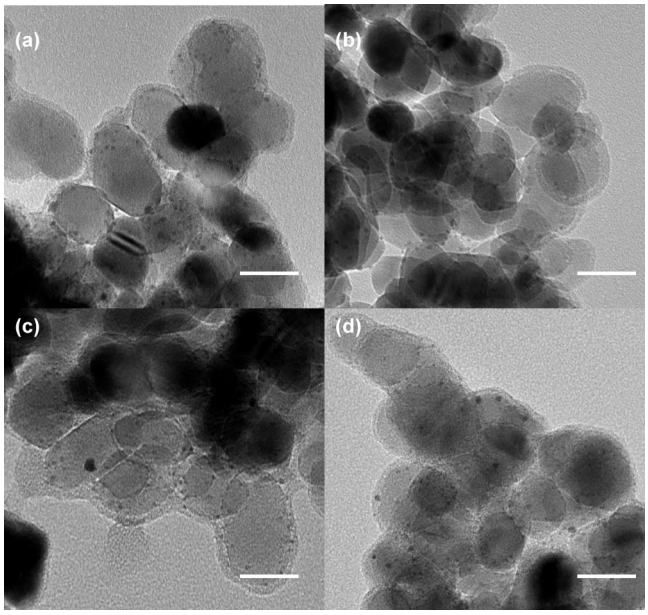

Figure 4. TEM images of (a) Poly/Pt/TiO_2(1), (b) Poly/Pt/TiO_2(2.5), (c) Poly/Pt/TiO_2(12), and (d) Poly/Pt/TiO_2(30). Scale bars correspond to 20 nm.

species regardless of photoirradiation time.[13] Overall enhancement in intensities of these absorption bands with increase in the duration of photoirradiation suggested an increase in the amount of polymer accumulated on the surface of TiO_2. Since these absorption bands are characteristics of a phenolic polymer,[14] the polymer covering the surface of TiO_2 was confirmed to have resulted from polymerization of phenol, as was analogized from the above TG analyses.

Figure 4 shows TEM images of Poly/Pt/TiO_2 samples after photoirradiation for 1, 2.5, 12, and 30 h. After photoirradiation for 1 h, the entire surface of TiO_2 was surrounded by a thin polymer layer (ca. 3 nm in thickness), indicating that complete coverage of a phenolic polymer on TiO_2 was achieved by photoirradiation for even such a short duration (Figure 4a). Moreover, the fact that Pt nanoparticles were observed as small black dots between the polymer layer and TiO_2 in the TEM images displays successful photoreduction of H_2PtCl_6 by TiO_2 during photoirradiation.

The thickness of the polymer layers in Poly/Pt/TiO_2 particles obtained after various durations of photoirradiation was determined from TEM images shown in Figure 4 by measuring more than 200 Poly/Pt/TiO_2 particles.[15] As a result, despite the monotonic increase in the amount of the polymer with the duration of photoirradiation (see above), the thickness of the layers was almost constant between these Poly/Pt/TiO_2 samples (ca. 3 nm). These results strongly suggest the occurrence of densification of the surface-covered polymers during prolonged photoirradiation.

Since the high oxidation potential of photogenerated h^+ in TiO_2 leads to complexity of the phenol polymerization process, the exact chemical pathway during densification of phenolic polymer is not understood at present. However, when a reaction pathway of the electrochemical oxidative phenol polymerization reported by Grattrell and Kirk was applied to the present system,[16] positive h^+ generated on TiO_2 was initially used to oxidize phenol into phenoxy radicals, and these radical species coupled with other phenols to form dimer, oligomer, and polymer radicals. As discussed in our previous paper,[10] the existence of such C−O and C−C coupling processes was evident from the presence of phenoxyphenol and biphenyl in the reaction suspension after 10 min photoirradiation. Because of the insolubility of these elongated phenolic species in aqueous solution, they attached to and probably self-terminated on the surface of TiO_2, resulting in the formation of a coarsely covered polymer layer on TiO_2. Once the entire surface of TiO_2 was covered by such a layer after a short duration of photoirradiation, the subsequent polymerization process did not lead to the formation of a multilayer polymer coating that would increase the thickness of the polymer layer, as shown in Figure 4. A possible model to explain the above results is that free phenol, which continuously penetrated the loosely packed polymer to reach the accessible surface sites of TiO_2, was photoexcited to form radical species followed by reaction with the surrounding polymer backbone to form a densified polymer layer. Because of the gradual densification during photoirradiation, penetration of fresh phenol into the polymer layer to reach the TiO_2 surface was gradually suppressed, leading to decrease in the rate of overall reaction, as has been observed in the time course of H_2 liberation (see Figure 1a).

Physical Properties of *n*Pt@*h*C Derived from Different Photoirradiation Times. A previous study has shown that the Poly/Pt/TiO_2 sample obtained after 2.5 h photoirradiation (Poly/Pt/TiO_2(2.5)) was converted into the *n*Pt@*h*C composite by carbonization of the polymer layer at 700 °C under vacuum followed by removal of the TiO_2 core particles by a chemical etching method using 50% aqueous HF.[10] Since the surface-covered polymers obtained by photoirradiation for various durations have different packing densities as described above, carbon shells derived from them are expected to have different properties. On the basis of this idea, the *n*Pt@*h*C composites were fabricated from these Poly/Pt/TiO_2 samples by the above-mentioned procedure. Figure 5 shows typical TEM images of samples thus obtained. All of the samples exhibited the same morphology regardless of duration of photoirradiation: hollow structured carbons encapsulating Pt nanoparticles. It is

(13) Peaks at 1230 and 1170 cm^{-1} in the FT-IR spectra of Poly/Pt/TiO_2 samples were ascribed to the asymmetric vibrations of the C−O−C bending and C−OH vibration, respectively. The presence of a benzene ring was verified by absorption bands at 1460, 1520, and 1620 cm^{-1} of the aromatic C−C stretching vibration. A C═O stretching band contributed from ester groups generated as a result of benzene ring-opening reaction or from benzoquinone groups produced as typical derivatives from phenol oxidation was also observed at 1720 cm^{-1}.

(14) (a) Gattrell, M.; Kirk, D. W. *J. Electrochem. Soc.* **1992**, *139*, 2736. (b) Lapuente, R.; Cases, F.; Garces, P.; Morallon, E.; Vazqueq, J. L. *J. Electroanal. Chem.* **1998**, *451*, 163.

(15) The thickness of the polymer layer in each Poly/Pt/TiO_2 sample was defined as the thin grayish layer covered on the relatively black TiO_2 particles in the TEM image.

(16) Gattrell, M.; Kirk, D. W. *J. Electrochem. Soc.* **1993**, *140*, 903.

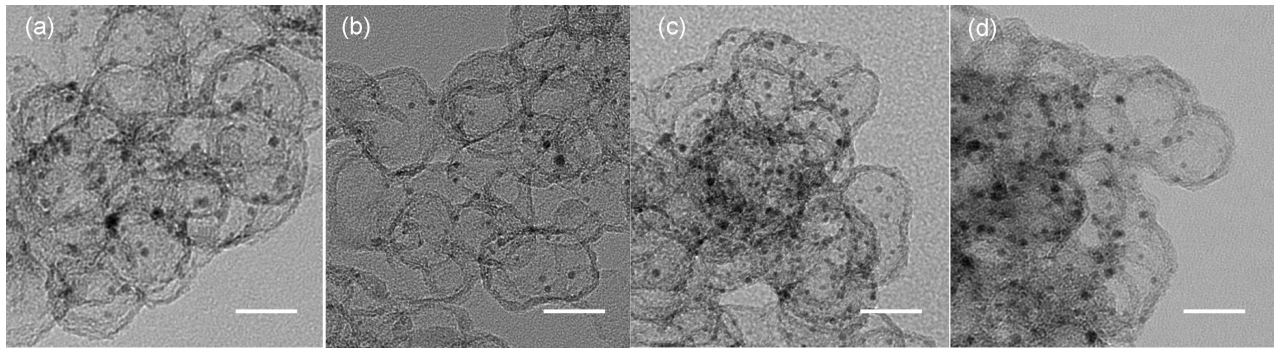

Figure 5. TEM images of (a) *n*Pt@*h*C(1), (b) *n*Pt@*h*C(2.5), (c) *n*Pt@*h*C(12), and (d) *n*Pt@*h*C(30). Scale bars correspond to 20 nm.

Table 1. Physical Properties of *n*Pt@*h*C Samples Derived from Various Durations of Photoirradiation

catalyst	T_{shell}[a]/nm (σ[b])	Pt [c]/nm (σ[b])	D_{ads}[d]/nm	D_{des}[e]/nm	W_{micro}[f]/nm	S_{BET}[g]/m^2 g^{-1}	V_{micro}[h]/cm^3 g^{-1}	Pt content[i]/wt %
*n*Pt@*h*C(1)	2.8 (0.68)	2.8 (0.58)	21	8.5	0.6	1320	0.43	3.3
*n*Pt@*h*C(2.5)	2.8 (0.63)	2.8 (0.60)	21	8.5	0.7	1080	0.35	1.5
*n*Pt@*h*C(12)	2.8 (0.82)	2.7 (0.58)	22	9.0	0.7	980	0.33	1.3
*n*Pt@*h*C(30)	2.8 (0.80)	2.7 (0.65)	22	9.0	0.7	690	0.23	1.0

[a] Thickness of carbon shell. [b] Standard deviation. [c] Pt size. [d] Diameter of mesopore from adsorption branch of isotherm. [e] Diameter of mesopore from desorption branch of isotherm. [f] Micropore width. [g] BET surface area. [h] Micropore volume calculated using HK formalism. [i] Pt content determined by ICP analysis.

noted that both thickness of the carbon shells and particle size of Pt nanoparticles calculated by measuring more than 200 *n*Pt@*h*C samples in randomly selected regions in these TEM images (Table 1) were comparable among these samples. The constant thickness of these shells indicates the densification of carbon components took place upon photoirradiation. In addition, the fact that the diameters of void spaces in these samples are almost the same as that of TiO_2 used proves inversely replication of TiO_2 templates for the formation of the present hollow carbon structure.

Figure 6 shows Ar sorption isotherms of *n*Pt@*h*C derived from various photoirradiation times. All the isotherms are categorized into type IV and show large hysteresis loops appeared from relative pressure (P/P_0) 0.4−0.9. This feature is typical for mesoporous materials having large pore sizes with narrow size distributions. Their corresponding pore size distributions determined from the BJH method from the adsorption data and the desorption data exhibit two different peaks centered at 21–22 and 8.5–9.0 nm, respectively (Figure S1 of Supporting Information). As reported previously,[10] the former corresponded to the diameter of void spaces of *n*Pt@*h*C, where the TiO_2 particles originally existed (see above). The latter is likely to appear by the presence of the window, i.e., an interconnected channel within the *n*Pt@*h*C particles, as has been typically observed in mesocellular materials with foamlike morphologies which consist of aggregates of hollow spheres.[17] The formation of such a window in the present *n*Pt@*h*C sample originated from the aggregated form of the TiO_2 mold. Besides these mesoporosities in *n*Pt@*h*C samples, steep increases in Ar uptake at $P/P_0 < 0.1$ in these isotherms show the existence

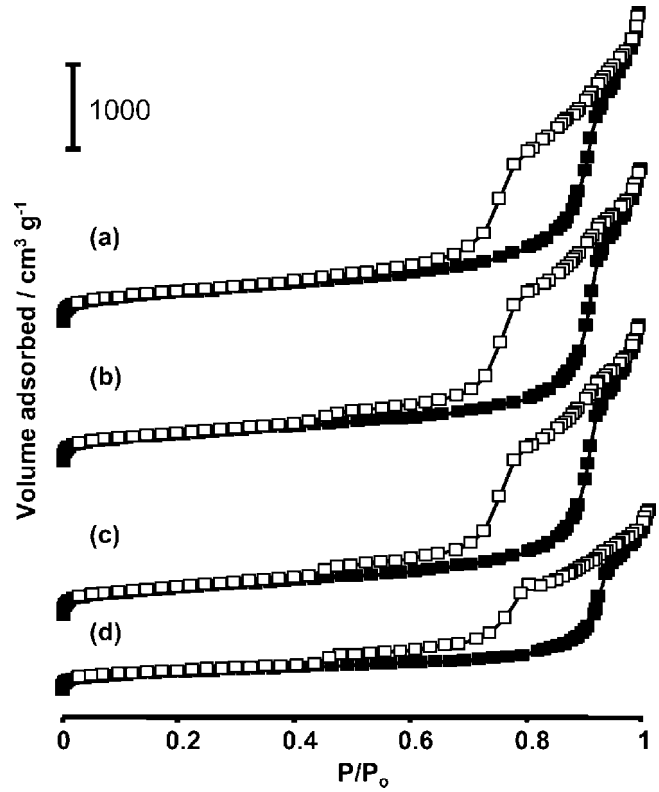

Figure 6. Ar sorption isotherms of (a) *n*Pt@*h*C(1), (b) *n*Pt@*h*C(2.5), (c) *n*Pt@*h*C(12), and (d) *n*Pt@*h*C(30). Filled and open squares denote adsorption and desorption branches, respectively.

of micropores inside the carbon shells. Indeed, micropore size distributions calculated by using the HK formalism indicate appreciable peaks centered at ca. 0.6–0.7 nm (Figure S2).

The structural parameters deduced from these isotherms are listed in Table 1 together with other physical properties obtained from different techniques. The mesopore sizes exhibit insignificant difference between the *n*Pt@*h*C samples, as expected from their structural similarities

(17) (a) Schimidt-Winkel, P.; Lukens, W. W., Jr.; Ying, P.; Margolese, D. I.; Lettow, J. S.; Ying, J. Y.; Stucky, G. D. *Chem. Mater.* **2000**, *12*, 686. (b) Lettow, J. S.; Han, Y. J.; Schmidt-Winkel, P.; Yang, P.; Zhao, D.; Stucky, G. D.; Ying, J. Y. *Langmuir* **2000**, *16*, 8291. (c) Oda, Y.; Fukuyama, K.; Nishikawa, K.; Namba, S.; Yoshitake, H.; Tatsumi, T. *Chem. Mater.* **2004**, *16*, 3860.

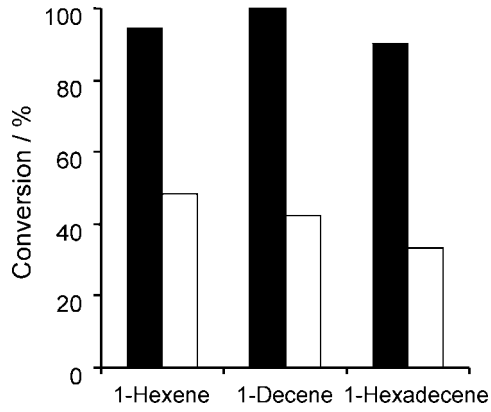

Figure 7. Liquid-phase hydrogenation of olefins catalyzed by *n*Pt@*h*C(1) (black blocks) and *n*Pt@*h*C(30) (white blocks) at ambient temperature and pressure.

observed in TEM images (Figure 5). Moreover, there is also no significant difference of the micropore sizes in these samples. Nevertheless, their BET surface areas and micropore volumes show appreciable differences between these samples: both of them monotonically decreased with increase in duration of photoirradition during the formation of Poly/Pt/TiO_2 samples. Hence, change in the density of the polymer layer in Poly/Pt/TiO_2 induced by duration of photoirradiation strongly influences the density of the resulting carbon shell in *n*Pt@*h*C without any alterations of pore sizes. These results imply that the densification of the carbon shell leads to filling of certain parts of the micropore systems inside the carbon shell to lose its microporosity. In addition, as a consequence of densification of the carbon shell, the content of Pt in the *n*Pt@*h*C sample gradually decreased with increase in duration of photoirradiation, as we expected.

Effect of Carbon Shell Densification of *n*Pt@*h*C on Its Catalytic Activity. Alteration in the porosity of support materials often has a significant influence in catalytic activity for several considerations, such as change in available surface area and modification of the diffusion mode for substrate(s) and product(s).[18] From this viewpoint, effects of densification of the carbon matrix in the present *n*Pt@*h*C sample on its catalytic function are one of the attractive subjects. Thus, we evaluated catalytic activities for hydrogenation of some normal olefins using *n*Pt@*h*C(1) and *n*Pt@*h*C(30) samples having the lowest and highest densities of carbon shell among the present samples, respectively. Figure 7 shows representative results of hydrogenation of 1-hexene, 1-decene, and 1-hexadecene over these samples. It is clear that remarkable activity is achieved with *n*Pt@*h*C(1): almost all of the substrates are converted into their corresponding normal alkanes by *n*Pt@*h*C(1), whereas the reactions do not go to completion with *n*Pt@*h*C(30) under the present reaction condition. It should be noted that we confirmed the reusability of *n*Pt@*h*C(1) for the hydrogenation of 1-decene for at least three runs of reactions without significant loss of catalytic activity (data not shown). A TEM image of *n*Pt@*h*C(1) taken after the reaction revealed that there is no change in the structure of the catalyst (Figure S3).

The above results clearly indicate significant effects of carbon densification on the catalytic activity of the *n*Pt@*h*C composites. From cross-sectional imaging of an *n*Pt@*h*C sample in our different study,[19] we found that the Pt nanoparticles were actually embedded in the matrix of the carbon shell instead of being "rattled" inside the hollow structure. Therefore, one of the most possible explanations for the reduction of catalytic activity on the *n*Pt@*h*C(30) sample is the surface coverage of Pt nanoparticles by the growing carbon shell, leading to decrease in available active site(s). Actually, CO adsorption analyses of *n*Pt@*h*C(1) and *n*Pt@*h*C(30) at room temperature indicate that Pt dispersion (CO_{irr}/Pt), i.e., the ratio of surface Pt atoms available for CO adsorption to the total number of Pt atoms, of *n*Pt@*h*C(30) (CO_{irr}/Pt = 0.21) is smaller than that of *n*Pt@*h*C(1) (CO_{irr}/Pt = 0.36). Because the sizes of Pt nanoparticles in both samples are almost the same (Table 1), it is likely that the decrease in Pt dispersion is directly related to the decrease in active site(s) for the present catalytic reaction.

Besides the surface coverage of Pt nanoparticles with the carbon layer which act as a physical barrier between substrate(s) and Pt catalyst, decrease in micropore volume in the dense carbon shell prepared from longer irradiation time might limit the rate of substrate diffusion. Therefore, another probable explanation for the activity drops in the *n*Pt@*h*C(30) sample is that the dense carbon layer in *n*Pt@*h*C(30) obstructs permeation of the substrate through it to reach to the Pt catalysts. However, since other structural parameters in porosity such as micropore and mesopore sizes are almost comparable between *n*Pt@*h*C(1) and *n*Pt@*h*C(30) samples (Table 1) and since reactions of normal olefins employed in the present study should not provide clear size dependence, such effects of substrate diffusion have not yet proved. Hence, further investigations to identify factors determining the overall rate using various bulky substrates in different catalytic systems are now in progress.

Conclusion

In this study, a photocatalytic method for fabrication of hollow carbon encapsulating Pt nanoparticles was investigated, focusing on control of structural characteristics of the carbon shell. We proved that the density of the phenolic polymer, a carbon precursor, could be controlled by changing duration of photoirradiation during the deposition of Pt metal and the polymer onto TiO_2 particles, leading to tunability of density and porosity of the resulting hollow carbon shell. Moreover, the densification of carbon was found to reduce number of active surfaces on Pt nanoparticles, resulting in changes in catalytic activity of Pt for hydrogenation of olefins

(18) (a) Viswanadham, N.; Dixit, L.; Gupta, J. K.; Garg, M. O. *J. Mol. Catal. A: Chem.* **2006**, *258*, 15. (b) Arino, M.; Pinna, F.; Strukul, G. *Appl. Catal. B: Environ.* **2004**, *53*, 161.

(19) Pt nanoparticles were found to be embedded in the carbon shell. The carbon matrix kinetically locked the motion of Pt nanoparticles, resulting in remarkable thermal stability. The results will be submitted elsewhere.

with H_2. Because of its simplicity, the present strategy can be used as a tool for tuning properties of carbon-based materials when appropriate photocatalyst particles are employed.

Acknowledgment. Y. H. Ng is grateful for the scholarship from the Ministry of Education, Culture, Sports, Science, and Technology (MEXT), Japan. This work was supported by a Grant-in-Aid for Scientific Research on Priority Areas (No. 19028042, "Chemistry of Concerto Catalysis") from the Ministry of Education, Culture, Sports, Science and Technology, Japan. Professor Yoshito Tobe and Professor Keiji Hirose (Osaka University) are acknowledged for their stimulating suggestions and discussions.

Supporting Information Available: Mesopore and micropore size distributions of all *n*Pt@*h*C samples and TEM image of *n*Pt@*h*C composites after catalytic reaction. This material is available free of charge via the Internet at http://pubs.acs.org.

CM702034W